2025 IEEE International Women in Engineering (WIE) Conference on Electrical and Computer Engineering (WIECON-ECE)
21-22 December 2025, Cox's Bazar, Bangladesh

Machine Learning-Aided Microstrip Patch Antenna for Breast Tumor Detection Using Scattering Parameters

Ashifa Islam Shamme
Department of Electrical and Electronic Engineering
Khulna University of Engineering & Technology
Khulna-9203, Bangladesh
Email: ashifa54islam@gmail.com

Ashfak Yeafi
Department of Electrical and Electronic Engineering
Khulna University of Engineering & Technology
Khulna-9203, Bangladesh
Email: yeafiashfak@gmail.com

Md Shamim Ahamed
Department of Electrical and Electronic Engineering
Atish Dipankar University of Science & Technology
Dhaka-1230, Bangladesh
Email: shamimahmed201080@gmail.com

***Abstract*—Breast cancer remains a major cause of mortality among women, motivating accurate, low-cost, and non-invasive detection methods. Conventional imaging (mammography, Ultrasound, MRI) faces limitations such as ionizing radiation, high cost, and reduced performance in dense breasts. Microwave and millimeter-wave techniques offer a non-ionizing alternative by exploiting dielectric contrasts between healthy and malignant tissues. In this work, an inset-fed rectangular microstrip patch antenna operating at 33 GHz is designed in CST Studio Suite and integrated with a multilayer semi-spherical breast phantom modeled via the Cole–Cole dispersion model. Scattering parameters (S, Y, and Z) are extracted under tumor-present and tumor-absent conditions to construct three structured datasets. Machine learning models, including Logistic Regression (LR), Support Vector Machine (SVM), Random Forest (RF), and a soft-voting ensemble, are trained to distinguish tumor from non-tumor cases. The ensemble achieves accuracies of 98.0% (S), 97.8% (Z), and 97.5% (Y), outperforming individual classifiers and demonstrating the benefit of ML-based analysis of scattering parameters. The study serves as a simulation-based proof-of-concept. Future work will focus on antenna fabrication, measurements with tissue-equivalent phantoms, and enlarged datasets with varied tumor sizes and positions to assess real-world generalization.**

***Index Terms*—Microstrip patch antenna, Microwave imaging, Scattering parameters (S, Y, Z), Ensemble learning**

I. Introduction

Breast cancer remains a leading cause of cancer-related deaths among women worldwide, making early and reliable detection critically important [1]. Conventional screening techniques such as mammography, Ultrasound, CT, PET, and MRI have well-known drawbacks, including ionizing radiation, high cost, reduced sensitivity in dense or younger breasts, and limited portability [2]–[4]. These limitations have motivated the exploration of microwave and millimeter-wave (mmWave) imaging as safer, low-cost, and non-ionizing alternatives that exploit the dielectric contrast between malignant and healthy tissues [5]–[7].

In microwave-based breast imaging, the antenna is a key component, as it must efficiently couple energy into the breast and sense subtle perturbations in the scattered fields caused by a tumor. Microstrip patch antennas are attractive due to their compact size, low profile, and ease of integration. However, accurately interpreting measured scattering parameters (S, Y, and Z) to distinguish tumor-bearing from healthy tissues is challenging. Simple thresholding of $|S_{11}|$ or resonance shifts at a few frequencies often fails to capture the complex, non-linear and frequency-dependent behavior of the scattering response. Machine learning (ML) offers a data-driven alternative that can exploit joint information across frequency, magnitude, and phase to improve classification robustness [8].

Motivated by these considerations, this paper proposes a hybrid framework that integrates a 33 GHz microstrip patch antenna with a multilayer breast phantom and ML-based classification. Scattering parameters are extracted from full-wave simulations under tumor and non-tumor conditions to construct three structured datasets based on S-, Y-, and Z-parameters, each encoding frequency, magnitude, and phase information. Several classical ML models (LR, SVM, RF) and a soft-voting ensemble are then trained and evaluated to quantify how well each scattering domain supports tumor detection and to demonstrate the benefit of ML over simple threshold-based analysis. Compared to many existing antenna-based breast cancer studies, this work focuses on the mmWave regime and provides a systematic comparison of S, Y, and Z domains combined with multiple classifiers and an ensemble model in a unified framework.

The main contributions of this paper are summarized as follows:

- Design and simulation of a 33 GHz inset-fed microstrip patch antenna integrated with a multilayer breast phantom for microwave-based tumor detection.

- Construction of three structured datasets in S-, Y-, and Z-parameter domains, each including frequency, magnitude, and phase features derived from full-wave simulations.
- Development and evaluation of a machine learning pipeline incorporating LR, SVM, RF, and a soft-voting ensemble, demonstrating that ensemble learning significantly improves scattering-parameter-based tumor classification.

The remainder of this paper is organized as follows. Section II reviews related work on microwave-based breast tumor detection and ML approaches. Section III describes the proposed methodology, including antenna design, phantom modeling, dataset construction, and ML framework. Section IV presents the simulation and classification results with discussion. Section V provides concluding remarks and directions for future work.

II. Related Work

Microwave imaging has been extensively investigated as a non-ionizing and cost-effective alternative to conventional breast cancer screening modalities. The fundamental principle relies on the dielectric contrast between healthy and malignant tissues, which enables microwave signals to differentiate tumor regions. Various antenna structures, such as monopoles, Vivaldi antennas, and microstrip patches, have been proposed for breast tumor detection due to their wide bandwidth, compact design, and adaptability for biomedical use [9]–[11]. Ultra Wideband (UWB) microwave imaging offers a low-complexity, cost-effective, and accurate approach for early breast cancer detection. Operating within a 3.5–7.2 GHz frequency range, it demonstrates reduced signal reflection with larger tumors. Simulations indicate improved return loss with increased tumor size, and the design is most effective when tumors are within 2 cm of the breast surface. However, the study lacked detailed image quality evaluation and did not present specific performance metrics for tumor detection [12].

Early works employed simple homogeneous phantoms, but more recent studies have developed multilayer phantoms that mimic skin, fat, glandular, and tumor tissues with realistic dielectric properties [13], [14]. Studies have demonstrated that malignant tissues exhibit significantly higher dielectric permittivity and conductivity compared to normal tissues [15], [16], reinforcing the feasibility of microwave detection techniques.

Beyond antenna and phantom design, the classification of tumor presence from measured scattering parameters (S, Y, and Z) presents additional challenges. Traditional thresholding and handcrafted feature extraction approaches often fail to capture the complex, frequency-dependent behavior of scattering data. Recent advances in ML have shown promise in overcoming these limitations by enabling automated feature learning and robust classification. SVMs, RF, and neural networks have been successfully applied to microwave imaging tasks such as tissue classification and tumor localization [17]–[20]. Furthermore, the use of scattering parameters as features has shown encouraging results in related biomedical sensing applications, suggesting their potential utility for breast tumor detection [21]–[23].

In summary, prior research has demonstrated the effectiveness of microwave imaging and antenna-based systems, as well as the potential of ML methods in biomedical classification tasks. However, limited studies have directly integrated microstrip antenna-based scattering parameter measurements with machine learning pipelines trained on structured S, Y, and Z parameter datasets. This motivates the present work, which combines antenna design, phantom-based validation, and ML-driven classification to enhance the accuracy and interpretability of breast tumor detection.

TABLE I
Design Parameters of the Proposed Antenna

Parameter	Value
Substrate Length (SL)	4.7 mm
Substrate Width (SW)	4.7 mm
Substrate Height (SH)	0.508 mm
Patch Length (PL)	2.75 mm
Patch Width (PW)	3.1 mm
Conductor Thickness (Mt)	0.035 mm
Inset Gap (MW)	0.2 mm
Inset Length (inL)	0.2 mm
Inset Width (inW)	0.15 mm
Antenna–Phantom Separation	2 mm
Design Frequency (f_r)	33 GHz

III. Methodology

The proposed framework for breast tumor detection integrates a microstrip patch antenna operating at 33 GHz resonance frequency, a multilayer breast phantom model, scattering parameter extraction, and machine learning-based classification.

A. Antenna Design

An inset-fed rectangular microstrip patch antenna was designed to resonate at 33 GHz within the 30–40 GHz frequency band in CST Studio Suite. Perfect electric conductor (PEC) material was used for the patch and ground plane to simulate ideal metallic behavior with negligible losses for simplified analysis and optimal performance estimation, while Rogers RT5880 (lossy) substrate ($\varepsilon_r = 2.2$, $\tan\delta = 0.0009$) was selected for its low dielectric loss and stable performance in the millimeter-wave region. The antenna was optimized using an inset feed line to achieve impedance matching between the patch and the feed network, thus minimizing reflections at the input port. The design parameters of the proposed antenna are summarized in Table I, and the optimized structure is depicted in Fig. 1.

B. Breast Phantom Model

To emulate realistic tissue properties, a semi-spherical breast phantom was modeled consisting of skin, adipose tissue, and fibro-glandular tissue. A spherical tumor was embedded in the

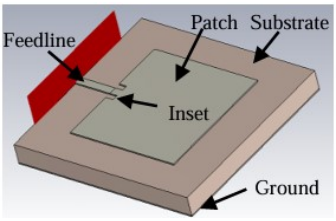

Fig. 1. Inset-fed rectangular microstrip patch antenna designed at 33 GHz.

TABLE II
DIELECTRIC PROPERTIES OF BREAST TISSUES AT 33 GHZ [24]

Tissue	Permittivity (ε')	Tangent Loss
Skin (with Areola)	17.7	0.93
Adipose Tissue	3.4	0.16
Fibro-glandular Tissue	16.0	0.96
Tumor (Maligant Tissue)	18.0	1.05

glandular layer. The phantom radius was set to 10 mm, with a skin thickness of 0.5 mm, adipose thickness of 0.5 mm, and glandular tissue occupying the remaining volume. Tumor diameters of 1 mm was considered. The phantom configuration with antenna placement is shown in Fig. 2.

The dielectric properties of tissues were modeled using the Cole–Cole dispersion model [24]:

$$\varepsilon_r(\omega) = \varepsilon_{ro} + \frac{\Delta\varepsilon_r}{1+(j\omega\tau)^{1-\alpha}} + \frac{\sigma_s}{j\omega\varepsilon_0} \tag{1}$$

where $\omega = 2\pi f$ is the angular frequency, τ is the relaxation time, $\Delta\varepsilon_r$ is the dielectric dispersion magnitude, ε_{ro} is the permittivity at optical frequencies, ε_0 is the permittivity of free space, α represents the dispersion broadening factor, and σ_s is the ionic conductivity. The tissue-specific dielectric parameters at 33 GHz are listed in Table II, confirming that malignant tissues exhibit higher permittivity and loss tangent than healthy tissues, which directly influences electromagnetic field propagation.

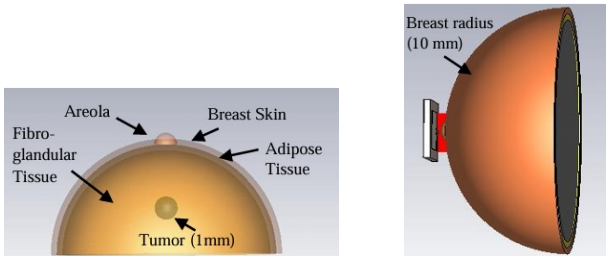

(a) Multilayer breast phantom

(b) Antenna placement with phantom

Fig. 2. (a) Semi-spherical breast phantom model with multilayer tissues and tumor inclusion (b) Proposed antenna in front of phantom.

C. Dataset Construction

Scattering parameters were extracted from the antenna–phantom system for both tumor-present and tumor-absent scenarios. The measured reflection coefficient (S_{11}) is related to the input impedance of the antenna by

$$S_{11} = \frac{Z_{\text{in}} - Z_0}{Z_{\text{in}} + Z_0} \tag{2}$$

where Z_{in} is the input impedance of the antenna and $Z_0 = 50\ \Omega$ is the characteristic impedance. From S_{11}, the corresponding admittance (Y_{11}) and impedance (Z_{11}) parameters were derived as

$$Y_{11} = \frac{1}{Z_{11}}, \quad Z_{11} = \frac{1+S_{11}}{1-S_{11}} Z_0 \tag{3}$$

Thus, three distinct datasets were constructed: (i) frequency with S_{11} magnitude and phase, (ii) frequency with Y_{11} magnitude and phase, and (iii) frequency with Z_{11} magnitude and phase. Each dataset contained 2002 samples labeled as 0 (normal) or 1 (tumor). A summary is provided in Table III.

TABLE III
SUMMARY OF CONSTRUCTED DATASETS

Dataset	Features	Samples
S-parameter	Frequency, $\lvert S_{11}\rvert$, $\angle S_{11}$	2002
Y-parameter	Frequency, $\lvert Y_{11}\rvert$, $\angle Y_{11}$	2002
Z-parameter	Frequency, $\lvert Z_{11}\rvert$, $\angle Z_{11}$	2002

It is important to emphasize that these 2002 samples are not arbitrarily generated synthetic vectors, but are obtained from dense frequency sweeps of a full-wave electromagnetic simulation of the physically based breast phantom under tumor and non-tumor conditions. While this yields a relatively modest dataset size compared to large image databases, each sample encodes rich frequency-dependent magnitude and phase information. Extending the dataset to additional tumor sizes, positions, and more heterogeneous tissue configurations is reserved for future experimental studies.

D. Machine Learning Framework

The constructed datasets were processed using a machine learning framework to classify tumor and non-tumor conditions. Preprocessing involved z-score normalization followed by stratified partitioning into 80% training and 20% testing subsets, ensuring that the class balance was preserved in both sets. LR, SVM with radial basis function kernel, and RF classifiers were individually implemented to establish baseline performance. These models capture different levels of complexity: LR provides a linear baseline, SVM models non-linear margins in a kernel-induced feature space, and RF captures complex interactions via ensembles of decision trees. Furthermore, a soft-voting ensemble classifier was employed, which combines the probabilistic outputs of LR, SVM, and RF. This approach exploits the complementary strengths of each model, thereby enhancing overall robustness and improving classification accuracy.

The classification performance was evaluated using accuracy, precision recall, F1-score, and probabilistic measures

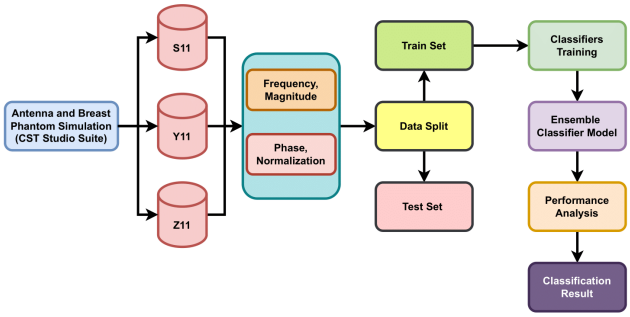

Fig. 3. Machine learning pipeline for scattering parameter-based tumor classification.

including the ROC and PR analysis. The fundamental metrics are defined as

$$\text{TPR} = \frac{\text{TP}}{\text{TP}+\text{FN}}, \qquad \text{FPR} = \frac{\text{FP}}{\text{FP}+\text{TN}}, \tag{4}$$

$$\text{Precision} = \frac{\text{TP}}{\text{TP}+\text{FP}}, \qquad \text{Recall} = \frac{\text{TP}}{\text{TP}+\text{FN}}. \tag{5}$$

The F1-score is given by

$$\text{F1-score} = 2 \cdot \frac{\text{Precision} \cdot \text{Recall}}{\text{Precision} + \text{Recall}}. \tag{6}$$

The ROC curve corresponds to TPR versus FPR across varying thresholds, while the PR curve corresponds to Precision versus Recall. In this work, only the scalar measures area under the ROC curve (ROC-AUC) and area under the PR curve (PR-AUC) are reported, as they effectively summarize classifier performance across all thresholds. Confusion matrices were also analyzed to identify classification strengths and misclassifications. The overall ML pipeline is illustrated in Fig. 3.

IV. Results and Discussion

A. Antenna Simulation Results

The proposed antenna was analyzed under three conditions: phantom with tumor, phantom without tumor, and no phantom (antenna in free space). The electromagnetic response was investigated in terms of return loss (S), admittance (Y), and impedance (Z) which is plotted in Origin Software, as shown in Fig. 4. These results highlight the impact of breast tissue dielectric loading and tumor presence on antenna performance. Fig. 4(a) shows the simulated S_{11} magnitude. For the tumor-absent phantom, the antenna resonates near 34.5 GHz with a return loss below -25 dB, confirming excellent impedance matching. The tumor-present phantom exhibits a slight resonance shift with reduced notch depth (-23 dB), demonstrating the sensitivity of the antenna to dielectric perturbations caused by malignant tissue. The no-phantom case exhibits a significantly different profile with a shallower notch around 33 GHz, highlighting the strong influence of tissue loading on reflection behavior. The Y_{11} response in Fig. 4(b) provides additional insight. Both tumor-present and tumor-absent phantoms produce admittance peaks in the 34–35 GHz range, with the tumor-present case exhibiting a slightly lower peak magnitude than the tumor-absent condition. In contrast, the no-phantom case results in a reduced admittance curve, emphasizing the stronger energy absorption introduced by biological tissue. The impedance magnitude Z_{11}, shown in Fig. 4(c), further confirms these observations. The tumor-absent phantom produces a minimum impedance of about 50 Ω, consistent with ideal antenna matching. The tumor-present phantom shifts this minimum upward toward 60 Ω, indicating increased resistance due to tumor-induced dielectric variations. The no-phantom case shows a distinctly higher impedance across the band, reaffirming the necessity of phantom loading for accurate biomedical evaluation.

Overall, these results validate that S, Y, and Z parameters provide complementary perspectives on antenna–tissue interactions. While S_{11} is conventionally used for antenna design and validation, the variations observed in Y_{11} and Z_{11} due to tumor presence offer additional discriminative features. This justifies their inclusion as feature sets for the subsequent machine learning classification framework.

B. Machine Learning Classification Results

To evaluate tumor detectability, scattering parameters (S, Y, and Z) were extracted from both tumor and tumor-free breast phantom models. Each dataset consisted of 2002 samples, where frequency and parameter values (magnitude and phase) were combined to form the feature space. These datasets were used to train LR, SVM, RF, and a soft-voting ensemble classifier. Performance was assessed in terms of accuracy, precision, recall, F1-score, ROC-AUC, and PR-AUC. The results are summarized in Table IV. The soft-voting ensemble consistently outperformed individual models across all datasets, achieving the highest accuracy of 98.0% for S-parameters, 97.8% for Z-parameters, and 97.5% for Y-parameters. RF also delivered strong performance with accuracies above 96%. In contrast, SVM and LR achieved significantly lower accuracies, below 80% and 55%, respectively. This clear performance gap between simple linear modeling (LR), non-linear margin-based modeling (SVM), and tree/ensemble-based modeling (RF and VOTE-SOFT) indicates that the relationship between scattering parameters and tumor presence is highly non-linear. The use of ML, particularly ensemble learning, therefore provides a tangible benefit over simple thresholding of $|S_{11}|$ or single-frequency rules by effectively exploiting the joint information across frequency, magnitude, and phase to reduce misclassifications.

Fig. 5 presents the confusion matrices for different classifiers, showing that ensemble and RF models minimize false negatives, which is critical in biomedical diagnostics.

V. Discussion and Conclusion

The simulated 33 GHz inset-fed microstrip patch antenna shows good impedance matching, stable radiation, and clear sensitivity to dielectric variations between healthy and malignant tissues. The comparison among phantom with tumor, phantom without tumor, and no phantom confirms that breast

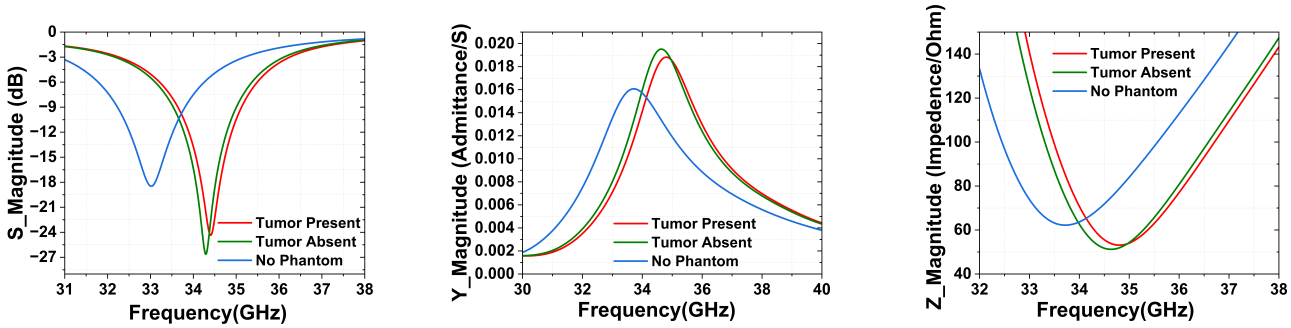

(a) S_{11} magnitude response (b) Y_{11} magnitude response (c) Z_{11} magnitude response

Fig. 4. Simulated antenna response under tumor-present, tumor-absent, and no-phantom conditions: (a) S_{11} magnitude, (b) Y_{11} magnitude, and (c) Z_{11} magnitude.

TABLE IV
CLASSIFICATION PERFORMANCE ACROSS DIFFERENT DATASETS AND MODELS

Dataset	Model	Accuracy	Precision	Recall	F1	ROC-AUC	PR-AUC
S	RF	96.5%	0.94	0.99	0.96	0.996	0.995
S	SVM	76.0%	0.75	0.77	0.76	0.79	0.80
S	LR	48.0%	0.47	0.44	0.45	0.46	0.45
S	VOTE-SOFT	**98.0%**	0.97	0.99	0.98	0.998	0.997
Y	RF	96.0%	0.93	0.985	0.96	0.980	0.978
Y	SVM	78.0%	0.75	0.77	0.76	0.79	0.80
Y	LR	50.0%	0.47	0.44	0.45	0.46	0.45
Y	VOTE-SOFT	**97.5%**	0.96	0.985	0.97	0.992	0.991
Z	RF	96.2%	0.935	0.988	0.96	0.982	0.980
Z	SVM	77.0%	0.75	0.77	0.76	0.79	0.80
Z	LR	52.0%	0.47	0.44	0.45	0.46	0.45
Z	VOTE-SOFT	**97.8%**	0.965	0.988	0.976	0.994	0.992

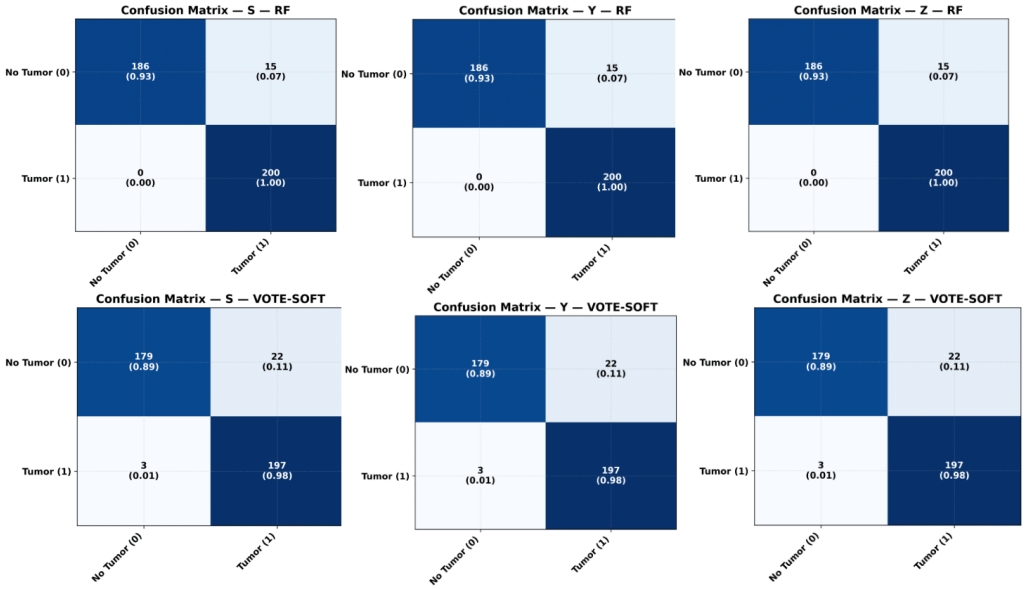

Fig. 5. Confusion matrices for S, Y, and Z parameter datasets across different classifiers.

tissue loading significantly alters the scattering response, justifying the use of S, Y, and Z parameters as indicators of tissue state.

From the ML perspective, all three scattering domains (S, Y, and Z) effectively detect tumor presence, with the soft-voting ensemble achieving accuracies of 98.0% (S), 97.8% (Z), and 97.5% (Y), and outperforming individual models such as LR and SVM. This performance gap indicates a highly non-linear relationship between scattering parameters and tumor presence and demonstrates the benefit of ensemble learning over simple thresholding of $|S_{11}|$ or single-frequency rules. Overall, the integration of a compact antenna with ML-based analysis yields a low-cost, non-ionizing, and accurate framework for breast tumor detection.

This study is purely simulation-based: the antenna and breast phantom are modeled in CST, and all datasets originate from a single tumor size and fixed phantom configuration. The results should therefore be viewed as a controlled proof-of-concept rather than a clinically validated system. Future work will focus on fabricating the antenna, performing measurements with tissue-equivalent phantoms, enlarging the dataset with varied tumor sizes and positions, and exploring deep learning models to further assess and improve real-world generalization.

REFERENCES

[1] A. N. Giaquinto, H. Sung, K. D. Miller, J. L. Kramer, L. A. Newman, A. Minihan, A. Jemal, and R. L. Siegel, "Breast cancer statistics, 2022," *CA: a cancer journal for clinicians*, vol. 72, no. 6, pp. 524–541, 2022.

[2] A. Yeafi, M. Islam, and M. S. U. Yusuf, "A deep learning framework for 3d brain tumor segmentation and survival prediction," *Healthcare Analytics*, p. 100418, 2025.

[3] A. Yeafi, M. Islam, S. K. Mondal, K. I. H. Nashad, and M. S. U. Yusuf, "A semi-supervised approach for brain tumor classification using wasserstein generative adversarial network with gradient penalty," in *2023 6th International Conference on Electrical Information and Communication Technology (EICT)*. IEEE, 2023, pp. 1–6.

[4] M. T. Jawad, A. Yeafi, and K. K. Halder, "Gsnet: a multi-class 3d attention-based hybrid glioma segmentation network," *Optics Express*, vol. 31, no. 24, pp. 40 881–40 906, 2023.

[5] R. Çalışkan, S. S. Gültekin, D. Uzer, and Ö. Dündar, "A microstrip patch antenna design for breast cancer detection," *Procedia-Social and Behavioral Sciences*, vol. 195, pp. 2905–2911, 2015.

[6] K. Ouerghi, N. Fadlallah, A. Smida, R. Ghayoula, J. Fattahi, and N. Boulejfen, "Circular antenna array design for breast cancer detection," in *2017 Sensors Networks Smart and Emerging Technologies (SENSET)*. IEEE, 2017, pp. 1–4.

[7] F. Bray, J. Ferlay, I. Soerjomataram, R. L. Siegel, L. A. Torre, and A. Jemal, "Global cancer statistics 2018: Globocan estimates of incidence and mortality worldwide for 36 cancers in 185 countries," *CA: a cancer journal for clinicians*, vol. 68, no. 6, pp. 394–424, 2018.

[8] W. Shao, "Machine learning in microwave medical imaging and lesion detection," *Diagnostics*, vol. 15, no. 8, p. 986, 2025.

[9] E. C. Fear and M. A. Stuchly, "Microwave breast imaging with a monostatic system," *IEEE Transactions on Microwave Theory and Techniques*, vol. 50, no. 11, pp. 123–131, 2002.

[10] X. Li, S. C. Hagness, and E. Bond, "An ultra-wideband vivaldi antenna and array for breast cancer detection," *Microwave and Optical Technology Letters*, vol. 38, no. 2, pp. 121–126, 2003.

[11] M. Klemm, I. J. Craddock, J. A. Leendertz, A. Preece, and R. Benjamin, "Radar-based breast cancer detection using a hemispherical antenna array—experimental results," *IEEE Transactions on Antennas and Propagation*, vol. 53, no. 8, pp. 2317–2323, 2005.

[12] E. Palantei, A. Amir, I. S. A. Dewiani, and A. Achmad, "Early stage cancer detection technique considering the reflected power from breast tissues," *ARPN Journal of Engineering and Applied Sciences*, vol. 10, no. 17, pp. 7361–7367, 2015.

[13] S. C. Hagness, A. Taflove, and J. E. Bridges, "Three-dimensional fdtd analysis of a pulsed microwave confocal system for breast cancer detection: Design of an antenna-array element," *IEEE Transactions on Antennas and Propagation*, vol. 47, no. 5, pp. 783–791, 1998.

[14] Z. Jiang, X. Li, E. J. Bond, and S. C. Hagness, "Phantom study and experimental results of a microwave imaging system for breast cancer detection," *IEEE Transactions on Biomedical Engineering*, vol. 52, no. 10, pp. 1911–1918, 2005.

[15] S. Gabriel, R. W. Lau, and C. Gabriel, "The dielectric properties of biological tissues: Iii. parametric models for the dielectric spectrum of tissues," *Physics in Medicine and Biology*, vol. 41, no. 11, pp. 2271–2293, 1996.

[16] W. T. Joines, Y. Zhang, C. Li, and R. L. Jirtle, "The measured electrical properties of normal and malignant human tissues from 50 to 900 mhz," *Medical Physics*, vol. 21, no. 4, pp. 547–550, 1994.

[17] P. M. Meaney, K. D. Paulsen *et al.*, "Microwave imaging for breast cancer detection: Advances in clinical testing," *IEEE Microwave Magazine*, vol. 13, no. 6, pp. 51–58, 2012.

[18] M. Pastorino, *Microwave Imaging*. John Wiley & Sons, 2010.

[19] A. Yeafi and L. Sarker, "Adtnet: Attention-guided u-net with dynamic cnn and transformers for skin cancer detection," in *2024 13th International Conference on Electrical and Computer Engineering (ICECE)*. IEEE, 2024, pp. 679–684.

[20] L. Sarker and A. Yeafi, "Ef-swinnet: A hybrid efficientnet-swin transformer model for skin cancer classification," in *2024 International Conference on Recent Progresses in Science, Engineering and Technology (ICRPSET)*. IEEE, 2024, pp. 1–4.

[21] B. M. Moloney, M. Ward, E. Jones, and M. Glavin, "Breast cancer detection using s-parameter features and artificial neural networks," *Progress In Electromagnetics Research*, vol. 49, pp. 45–63, 2014.

[22] A. Mirbeik and N. K. Nikolova, "Tumor detection using broadband microwave signals: Phantom experiments and machine learning approaches," *IEEE Transactions on Biomedical Engineering*, vol. 62, no. 7, pp. 1801–1811, 2015.

[23] J. Li, Y. Wang, and H. Chen, "Breast tumor classification using scattering parameters and machine learning methods," *Biomedical Signal Processing and Control*, vol. 65, p. 102358, 2021.

[24] C. Das, M. Z. Chowdhury, and Y. M. Jang, "A novel miniaturized mmwave antenna sensor for breast tumor detection and 5g communication," *IEEE Access*, vol. 10, pp. 114 856–114 868, 2022.